Supplementary Material

Boosting Urea Synthesis in Simulated Flue Gas Electroreduction by Adjusting W-W Electronic Properties

Xiao-hui Yao, [†a] Chang-yan Zhu, [†a] Jie Zhou,[a] Kun-hao Zhang,[b] Chun-yi Sun,[a] Man Dong,[a] Guogang Shan,*[a] Zhuo Wu,[a] Min Zhang,*[a] Xin-long Wang[a] and Zhong-min Su[c]*

[a]Key Laboratory of Polyoxometalate and Reticular Material Chemistry of Ministry of Education, National & Local United Engineering Laboratory for Power Battery Institution, Northeast Normal University, Changchun, Jilin, 130024, China E-mail: suncy009@nenu.edu.cn, shangg187@nenu.edu.cn, mzhang@nenu.edu.cn

[b]Shanghai Synchrotron Radiation Facility, 239 Zhangheng Road, Pudong New District, Shanghai, 200120, China

[c]State Key Laboratory of Supramolecular Structure and Materials, Institute of Theoretical Chemistry, College of Chemistry, Jilin University, Changchun, Jilin, 130024, China

Materials

The raw materials for Cu-$W_{18}O_{49}$-@ZIF-8 synthesis were purchased in Macklin. Other reagents and solvents applied in the synthesis and photocatalysis were purchased from Aladdin and Sigma-Aldrich.

Synthesis of Cu-$W_{18}O_{49}$@ZIF-8 composite

50 mg WCI_6 was dissolved in 10 mL of ethanol, which was vigorously stirred to obtain a yellow solution, then 6.88 mg $CuCl_2 \cdot 2H_2O$ was added to the solution. After further stirring for 10 min, the resultant solution was transferred to a 15 mL Teflon-lined autoclave, which was heated at 210 ℃, 12 h. After cooling down to room temperature, the grey-blue product was separated by centrifugation and washed with water and ethanol several times. The obtained product was dried in the vacuum overnight at 50 ℃. Then, 7.5 mg Cu-$W_{18}O_{49}$ and 81 mg dimethylimidazole were dispersed in 5 mL methanol, after stirring for 30 min, 5 mL methanol solution containing 36.66 mg $Zn(NO_3)_2 \cdot 6H_2O$ was added into the solution, which was further stirred for 45 min. The mixture was kept stationary for 2 hours at room temperature. The product was washed with water and methanol three times and dried in the vacuum overnight at 40 ℃.

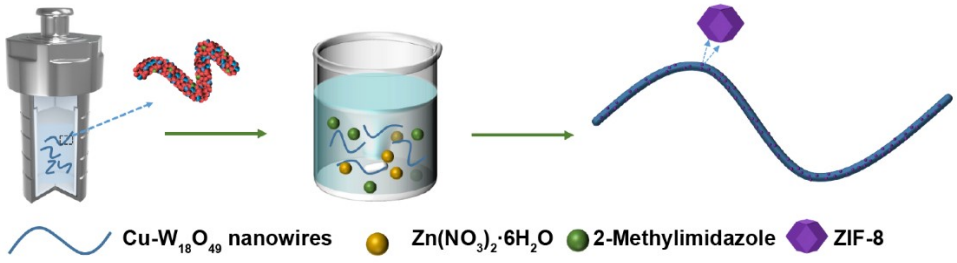

Scheme S1: Diagram of the preparation detail process for Cu-$W_{18}O_{49}$@ZIF-8 composite.

Characterization

A powder X-ray diffraction (PXRD) pattern was recorded by a Siemens D5005 diffractometer with Cu-Kα (λ = 1.5418 Å). ICP spectroscopy was conducted on Agilent 7500a Inductively Coupled Plasma Mass Spectrometry (ICP-MS 7500). TEM

images were recorded on a JEM-2010 transmission electron microscope at an accelerating voltage of 200 kV. UV-Vis absorption spectroscopy was obtained on a U-3900 spectrophotometer (Hitachi, Japan). Infrared spectra were obtained from KBr pellets in a wavelength ranging from 4000-400 cm^{-1} on a Nicolet 380 FT-IR spectrophotometer. XPS was performed using an Escalab 250 instrument. Nitrogen gas porosimetry measurements were performed on automatic volumetric adsorption equipment (ASIQM0G002-3) and a porosity analyzer after the samples were outgassed under a vacuum at 100 °C for 12 h. X-ray Absorption Near Edge Structure (XANES) and Extended X-ray Absorption Fine Structure (EXAFS) data were collected at Beamline 11B at Shanghai Synchrotron Radiation Facility (SSRF). In situ IR was carried out on a 6700 Flex FTIR spectrometer equipped with a smart iTRTM attenuated total reflectance (ATR) sampling accessory in the range of 500-4000 cm^{-1}.

Electrochemical measurements

Electrochemical measurement was carried out on a CHI660E electrochemical workstation in an H-cell with a three-electrode system. A Nafion 117 proton exchange membrane separated the H-type cell. The two compartments were filled with 0.25 M K_2SO_4 electrolyte. The as-prepared catalyst, platinum foil, and saturated Ag/AgCl electrode (filled with saturated KCl) acted as the working electrode, the counter electrode, and the reference electrode, respectively. To avoid contamination with nitrogen-containing species in the air, electrodes were used either immediately after preparation or kept in a vacuum before being used in electrochemical experiments. Potential without iR-compensated were converted to RHE scale via the following equation: E (vs. RHE) = E (vs. Ag/AgCl) + 0.0591 × pH + 0.197 (pH = 4.7 in CO_2-saturated electrolyte and N_2 + CO_2-saturated electrolyte in 0.25 M K_2SO_4; pH = 6.2 for N_2-saturated electrolyte in 0.25 M K_2SO_4). The catalyst ink for the working electrode was prepared by dispersing 10 mg of catalyst in a 1ml Nafion (0.5 wt% to sonication for 30 minutes. Mass loading of 0.4 mg cm^{-2} was used for the electrochemical study. All experiments were carried out at room temperature (25 ℃). To remove the impurities in the inlet gas, such as NO_x, the pre-purification of high-purity N_2 (purity 99.999%)

and CO_2 (purity 99.99%) by passing through a saturator filled with 0.05 M NaOH and a saturator filled with 0.05 M H_2SO_4 solution to remove any possible contaminants. Before carrying out all the electrochemical characterizations, the 0.25 M K_2SO_4 electrolyte solution was purged with CO_2 + N_2 for 30 minutes. In table S1, we summarized ink preparation process:

Table S1: Ink preparation proces

Catalyst quality	Nafion(5wt%)	H_2O	Ultrasound time	Ink concentration
e.g. Cu-$W_{18}O_{49}$@ZIF-8 10mg	0.1ml	0.9ml	30 minutes	10 mg/ml

Synthesis of H_2S and SO_x

100mg $Na_2S_2O_3$ was put in a 20 mL sealed headspace reaction bottle to prepare H_2S. The sealed headspace reaction bottle is connected to the gas-gathering device with a catheter and a needle. Next, 1mL 0.1 M H_2SO_4 was injected into the reactor with a 1 mL syringe, and the gas with the odor was generated and stored in a gas collection bag. For SO_x, replace $Na_2S_2O_3$ with $FeSO_4$, and inject 0.5 M H_2SO_4.

The concentrations of H_2S and SO_x is 0.2%, respectively.

Urea determination

The identification of urea was first achieved by the diacetyl monoxime method [1]. 500 mg of diacetylmonoxime (DAMO) and 10 mg of thiosemicarbazide (TSC) were dissolved in distilled water and diluted to 100 mL, denoted as DAMO-TSC solution. Then, 10 mL of concentrated phosphoric acid was mixed with 30 mL of concentrated sulfuric acid and 60 mL of distilled water, then 10 mg $FeCl_3$ was dissolved in the above solution, denoted as an acid-ferric solution. The preparation of the diacetyl monoxime colorant is summarized in Table S2. Typically, 1 mL of the sample solution was removed from the cathodic chamber. Afterward, 1 mL of DAMO-TSC solution and 2

mL of acid-ferric solution were added into 1 mL of sample solution. Next, the mixed solution was heated to 100 ℃ and maintained at this temperature for 15 min. When the solution cooled to 25 ℃, the UV-Vis absorption spectrum was collected at a wavelength of 525 nm. For high-performance liquid Chromatography spectroscopy. The quantification of urea was achieved by HPLC (SHIMADZU SPD-15C) spectroscopy. HPLC was performed on a Luna 5 μm NH_2 column (250 mm × 4.6 mm). The corresponding mobile phase, flow rate, and detected wavelength were acetonitrile-water (80:20), 0.2 mL min^{-1}, and 195 nm. For the ^1H NMR tests, dimethyl sulfoxided_6 (DMSO-d_6) was adopted as a deuterated reagent. First, 0.35 mL of extracted electrolyte without postprocessing was mixed well with 0.15 mL DMSO-d_6. Then, the liquid was transferred into the ^1H NMR tube for the test.

Table S2: Preparation of Diacetyl Monoxime Method Colorant.

DAMO-TSC solution	Diacetylmonoxime (DAMO)	Thiosemicarbazide (TSC)	H_2O
	500 mg	10 mg	100 ml
Acid-Ferric solution	Acid	$FeCl_3$	H_2O
	10ml phosphoric acid 30ml sulfuric acid	10 mg	60 ml

Determination of ammonia (NH_3):

The produced NH_3 was spectrophotometrically determined by the indophenol blue method [2]. Typically, 1 mL of the sample solution was removed from the cathodic chamber. Afterward, 1 mL of 1.0 M NaOH solution containing 5 wt% salicylic acid and 5 wt% sodium citrate was added, followed by 0.5 mL NaClO solution (0.05 M) and 0.1 mL of an aqueous solution of sodium nitroferricyanide (1 wt%) were added. After standing at room temperature for 2 hours, the UV-Vis absorption spectrum was collected at a wavelength of 655 nm.

Calculation of Faradaic efficiency (FE) and yield rate.

$$FE_{urea} = \frac{6 \times F \times C_{urea} \times V}{Q \times 60.06} \times 100\%$$

$$R_{urea} = \frac{C_{urea} \times V}{60.06 \times m_{cat} \times t}$$

$$FE_{NH_3} = \frac{3 \times F \times C_{NH_3} \times V}{Q \times 17} \times 100\%$$

$$R_{NH_3} = \frac{C_{NH_3} \times V}{17 \times m_{cat} \times t}$$

Where V is the electrolyte volume, C_{urea}/ C_{NH3} is the concentration of urea / NH_3, F is the Faraday constant, Q is the electric quantity, m_{cat} is the mass of the catalyst, t is the electrolysis time.

Computation Method

Spin-polarized density functional theory (DFT) [1-3] simulations were performed with the Vienna *ab initio* simulation package (VASP) [4]. The Perdew-Burke-Ernzerhof (PBE) functional within the generalized gradient approximation (GGA) and the projector augmented-wave (PAW) potential were employed [5,6]. The $W_{18}O_{49}$ (-101) facet was built from the optimized $W_{18}O_{49}$ bulk until cell with lattice parameters of a = 14.13 Å, b = 3.81 Å, c = 17.84 Å, β = 110.53°. The slab model consisting of 1 × 2 × 1 supercell was considered in this simulation, including 36 W atoms and 98 O atoms. Top two atom layers of this slabs were relaxed, while bottom two atom layers were fixed during optimization. The vacuum region of 15 Å was used in the vertical direction to the $W_{18}O_{49}$ surface to avoid superficial interactions between periodical

slabs. The plane-wave cutoff energy of 500 eV and the Monkhorst-Pack *k*-points mesh of 3 × 5 × 1 were adopted for all computations. The convergence criteria were set at 10^{-5} eV for total energy change and 0.05 eV $Å^{-1}$ for the maximum forces on each atom, respectively. The Grimme's semiempirical DFT-D3 method of dispersion correction was included to properly describe the vander Waals (vdW) interactions [7].The Gibbs free energy diagram and the adsorbed free energy during the electrocatalytic urea production were calculated using the computational hydrogen electrode (CHE) model developed by Nørskov et al [8,9].

.

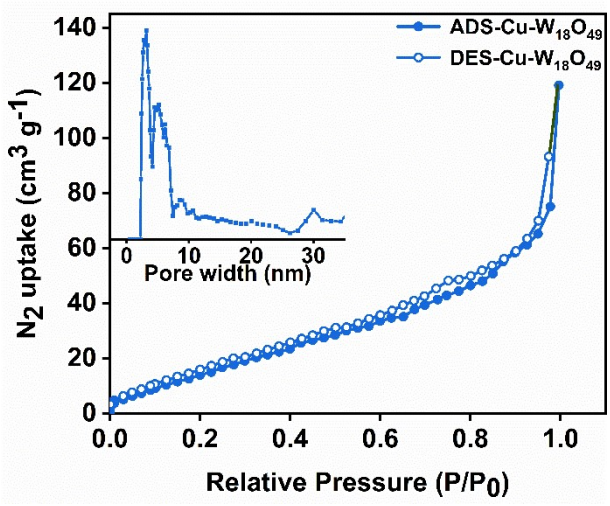

Fig. S1 Pore size distribution curve of Cu-$W_{18}O_{49}$.

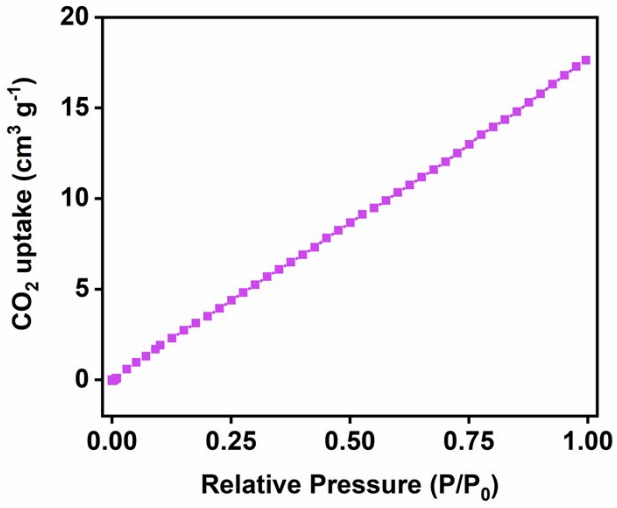

Fig. S2 CO_2 adsorption isotherm of Cu-$W_{18}O_{49}$@ZIF-8

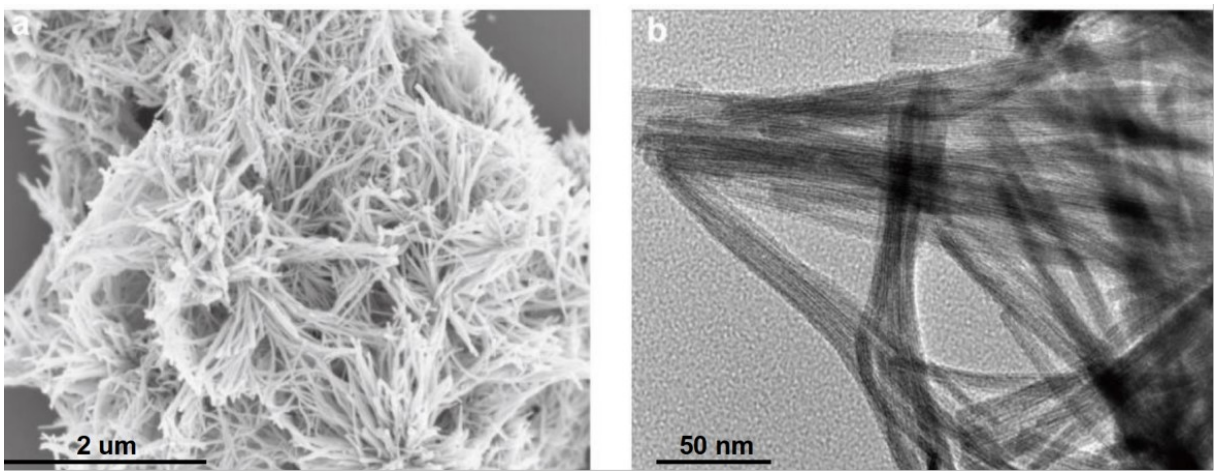

Fig. S3 SEM (a) and (b) image of Cu-$W_{18}O_{49}$.

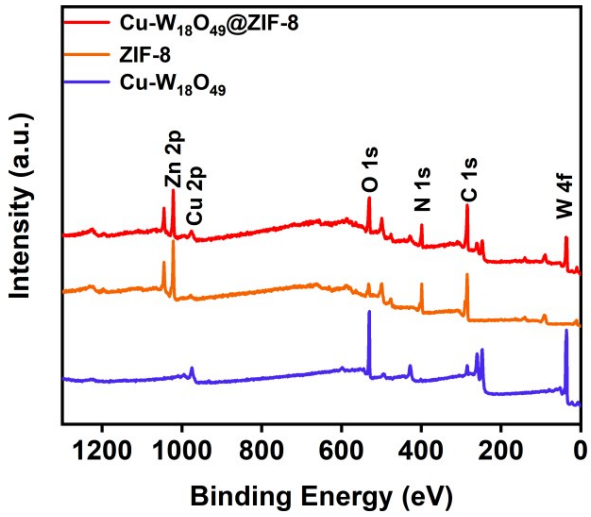

Fig. S4 XPS survey spectra of Cu-$W_{18}O_{49}$@ZIF-8.

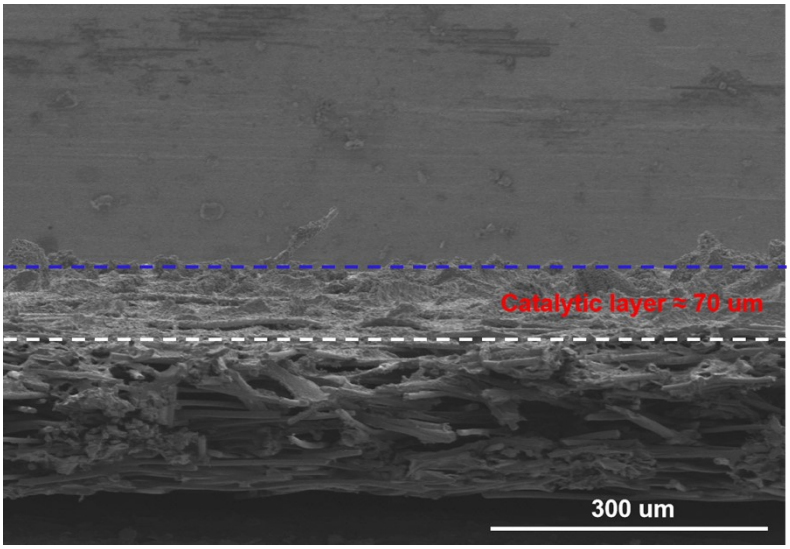

Fig. S5 SEM images of the thickness of the catalytic layer of the electrode.

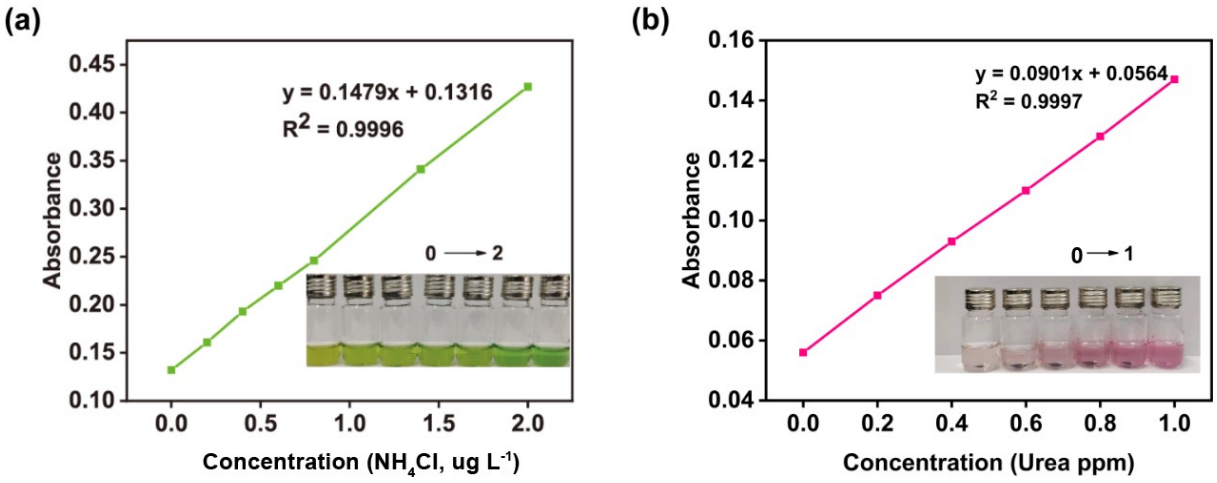

Fig. S6 (a) Concentration-absorbance of NH_4Cl solution with a series of standard concentration (0- 2 μg mL^{-1}) in 0.25 M K_2SO_4 and (b) Concentration-absorbance of urea solution with a series of standard concentration (0.2-1.0 μg mL^{-1}) in 0.25 M K_2SO_4.

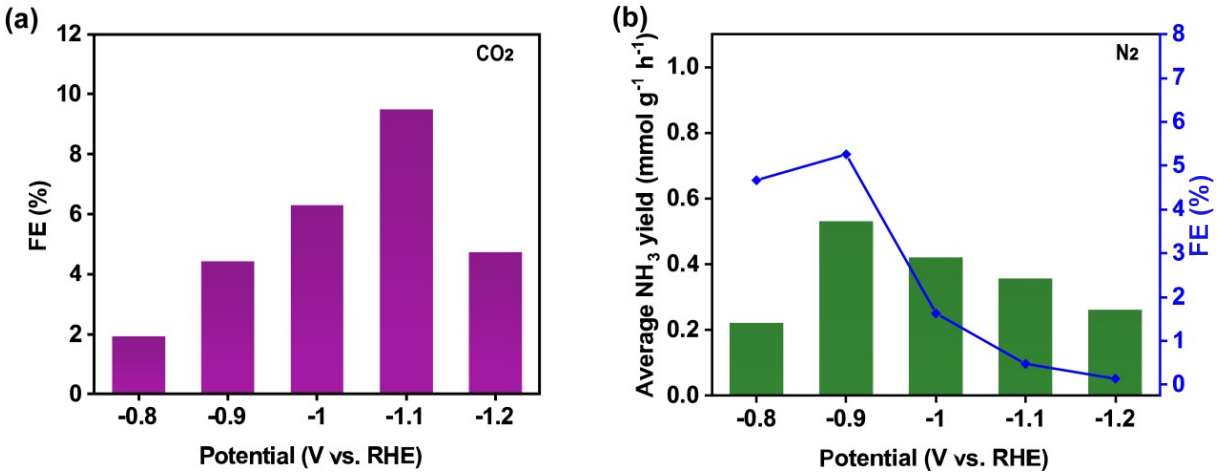

Fig. S7 (a) CO generate and (b) Ammonia product at various potentials for Cu-$W_{18}O_{49}$@ZIF-8.

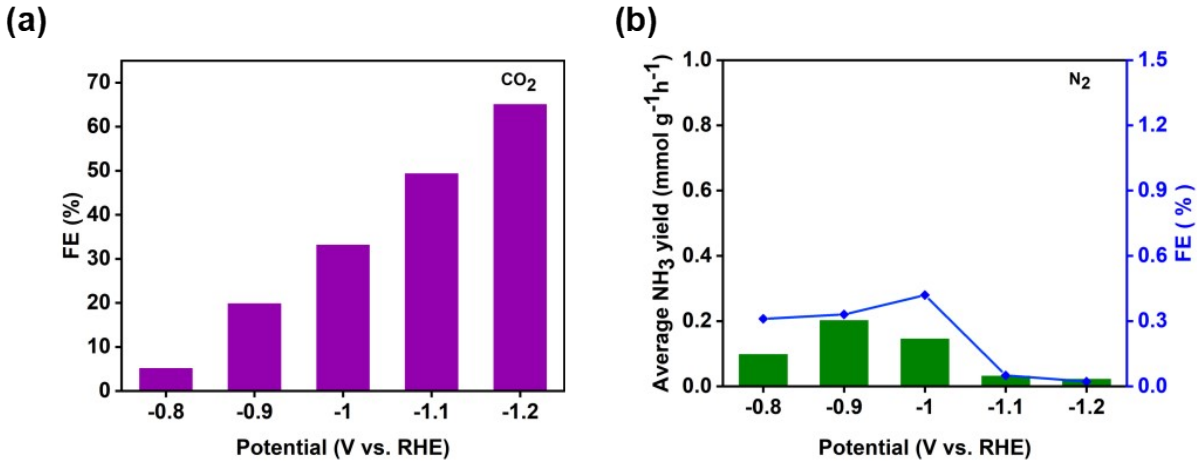

Fig.S8 (a) CO generate and (b) Ammonia product at various potentials for ZIF-8.

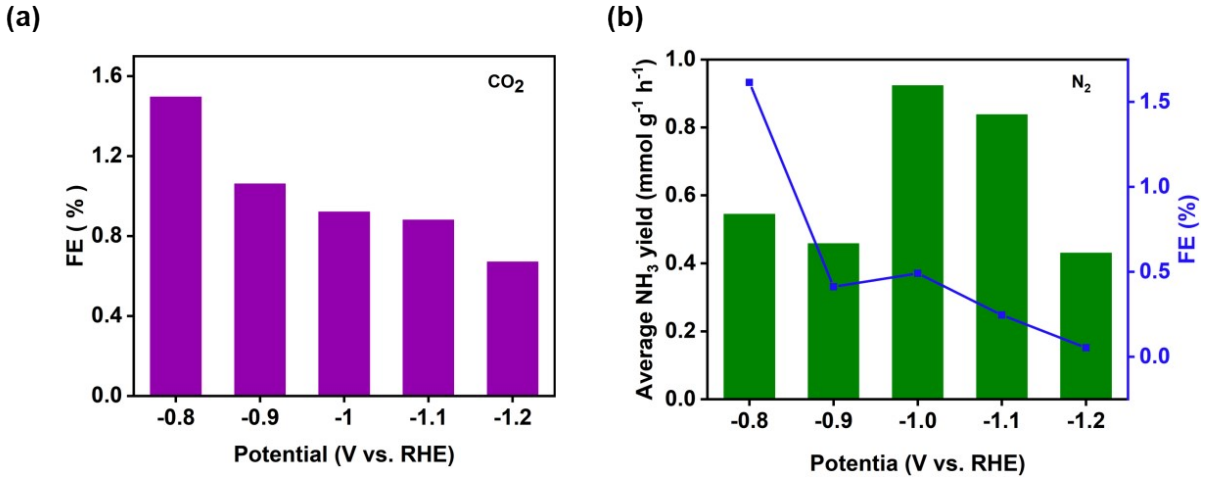

Fig. S9 (a) CO generate and (b) Ammonia product at various potentials for Cu-$W_{18}O_{49}$.

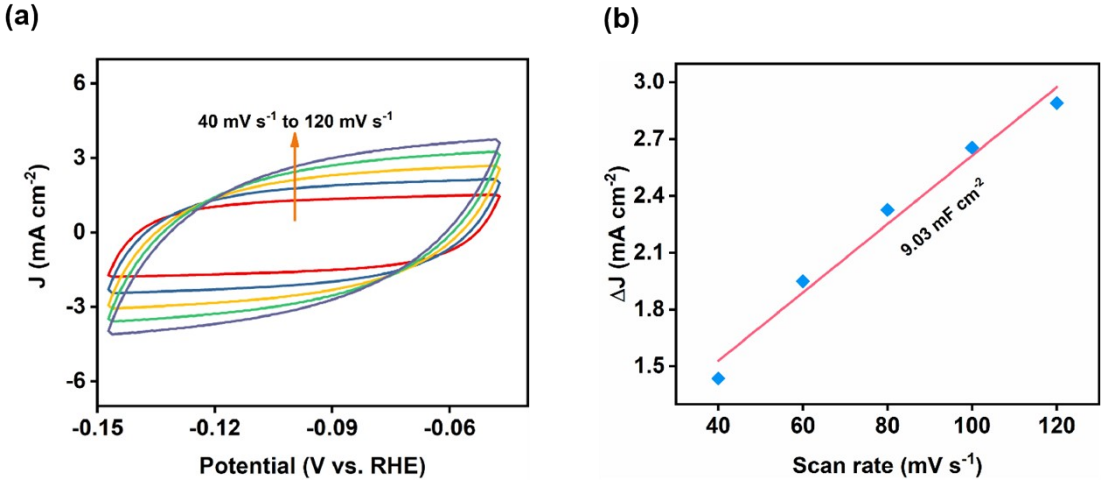

Fig.S10 (a) Different scan rate of Cu-$W_{18}O_{49}$@ZIF-8 (b) charging current density at different rates of Cu-$W_{18}O_{49}$@ZIF-8.

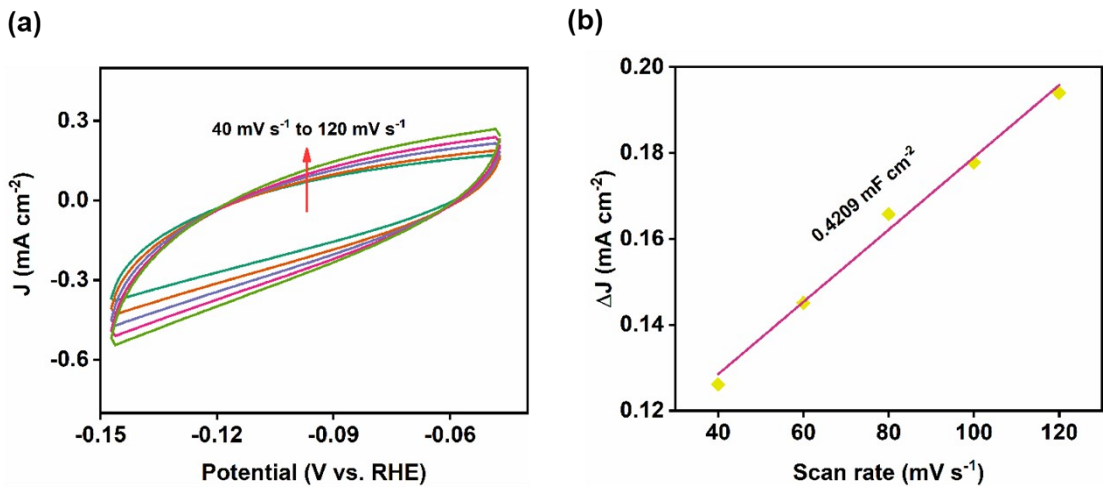

Fig. S11 (a) Different scan rate of $W_{18}O_{49}$@ZIF-8 (b) charging current density at different rates of $W_{18}O_{49}$@ZIF-8.

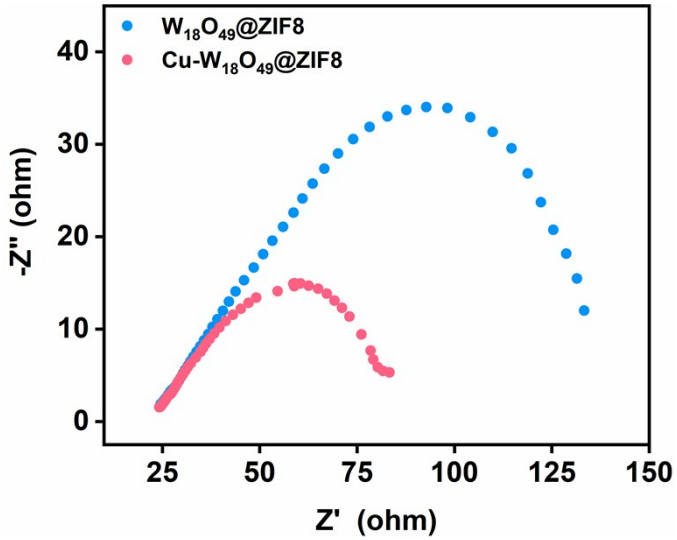

Fig. S12 Nyquist plots of $W_{18}O_{49}$@ZIF-8 and Cu-$W_{18}O_{49}$@ZIF-8.

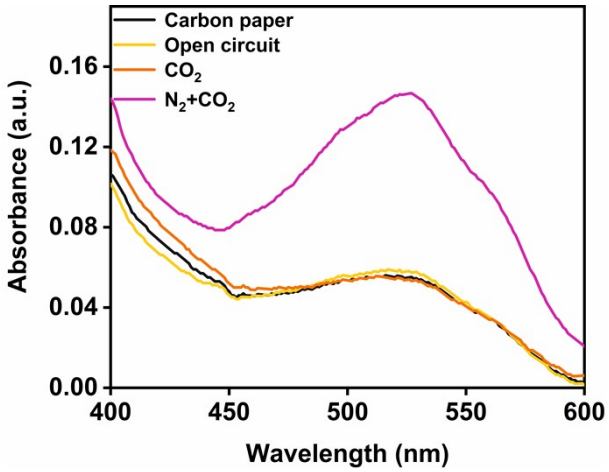

Fig. S13 The yield rate of urea under different reaction conditions (V_{N_2}: V_{CO_2}=3:1 at -1 V vs. RHE).

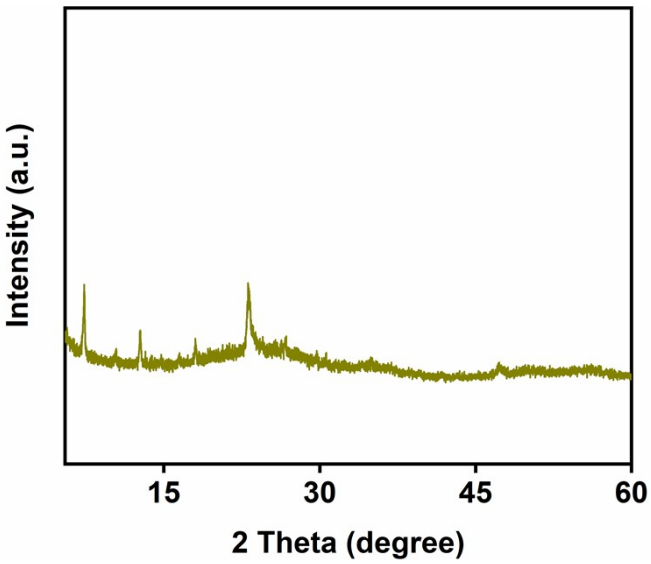

Fig. S14 XRD pattern of Cu-$W_{18}O_{49}$@ZIF-8 after electroreduction.

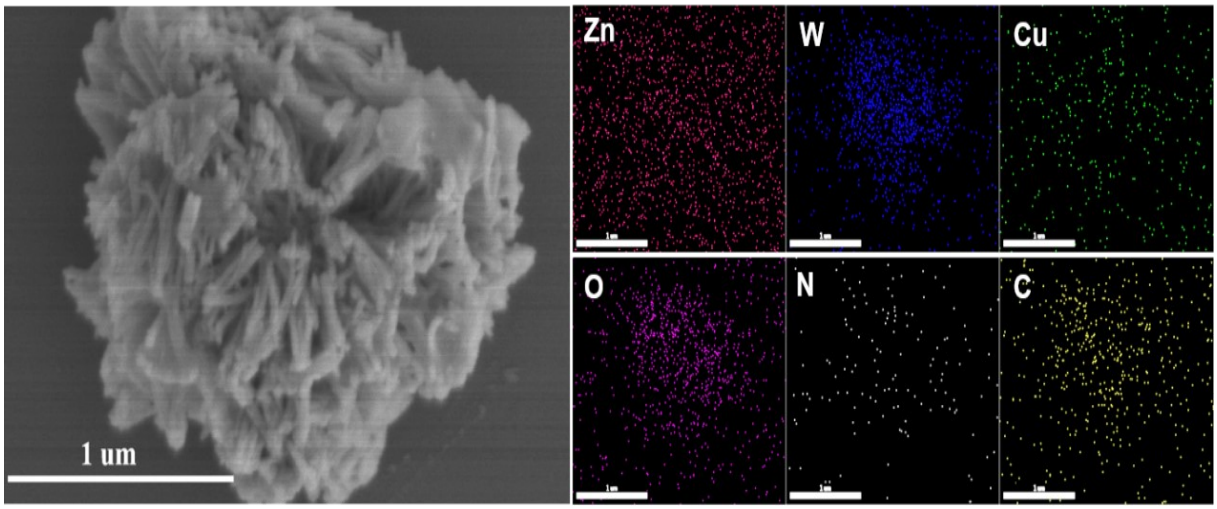

Fig. S15 SEM images of Cu-$W_{18}O_{49}$@ZIF-8 after electroreduction.

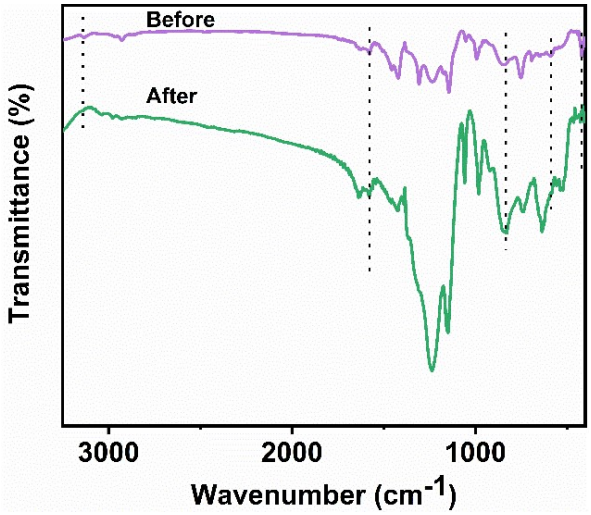

Fig. S16 FT-IR spectra of Cu-$W_{18}O_{49}$@ZIF-8 after electroreduction.

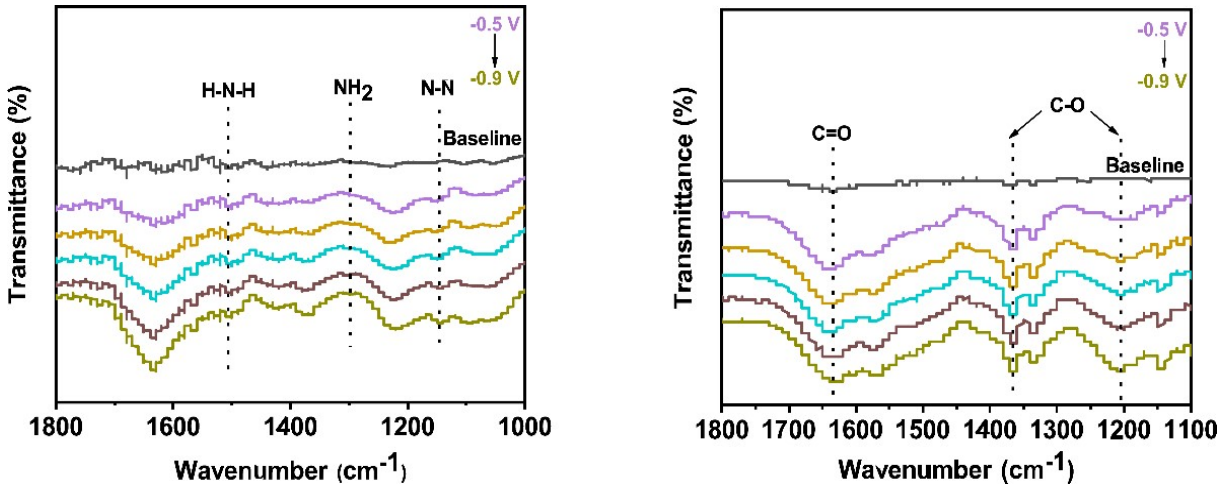

Fig. S17 In situ FT-IR spectra over Cu-$W_{18}O_{49}$@ZIF-8 with (a) N_2 and (b) CO_2 as the feeding gas.

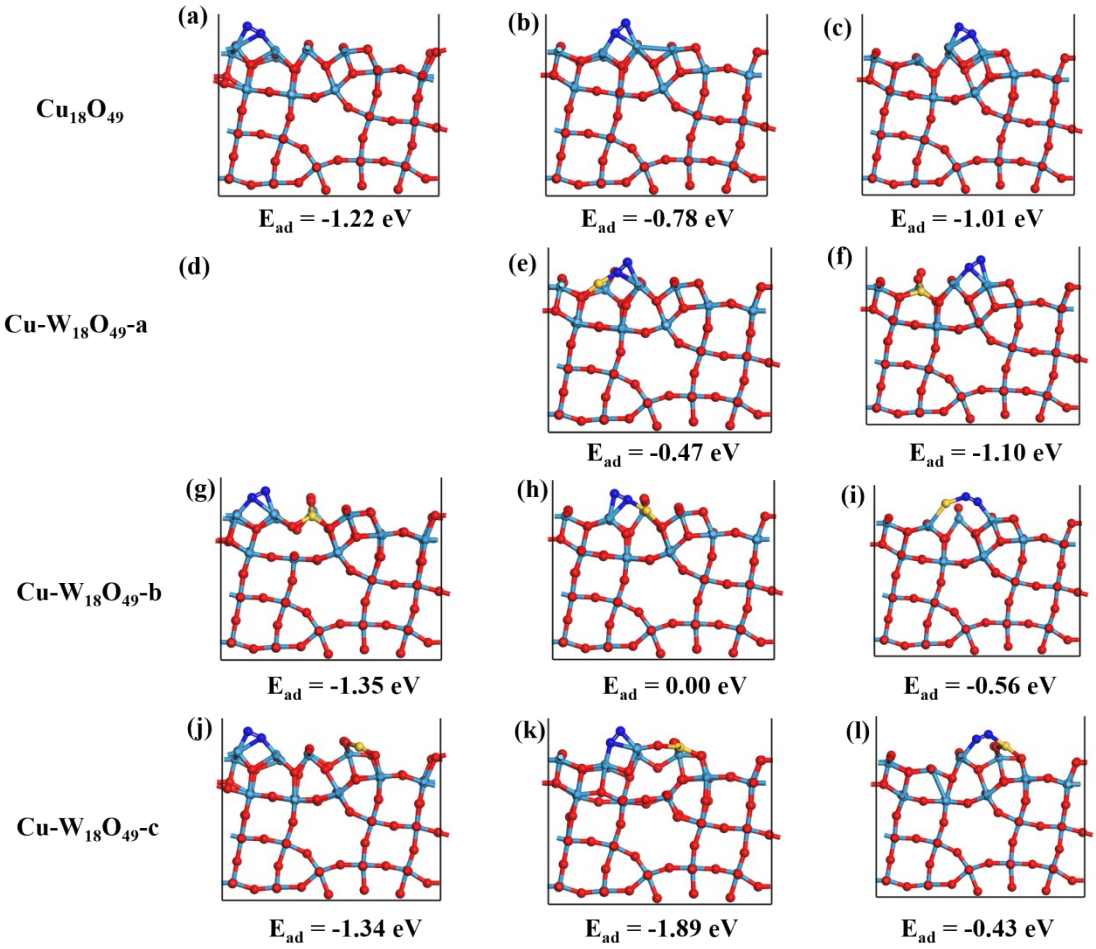

Fig. S18 Optimized structures and computed adsorption energies of *N_2 intermediates on the different catalytic sites of $W_{18}O_{49}$ and Cu-$W_{18}O_{49}$. Note that the *N_2 intermediate with side-on configuration in (d) can't be stable.

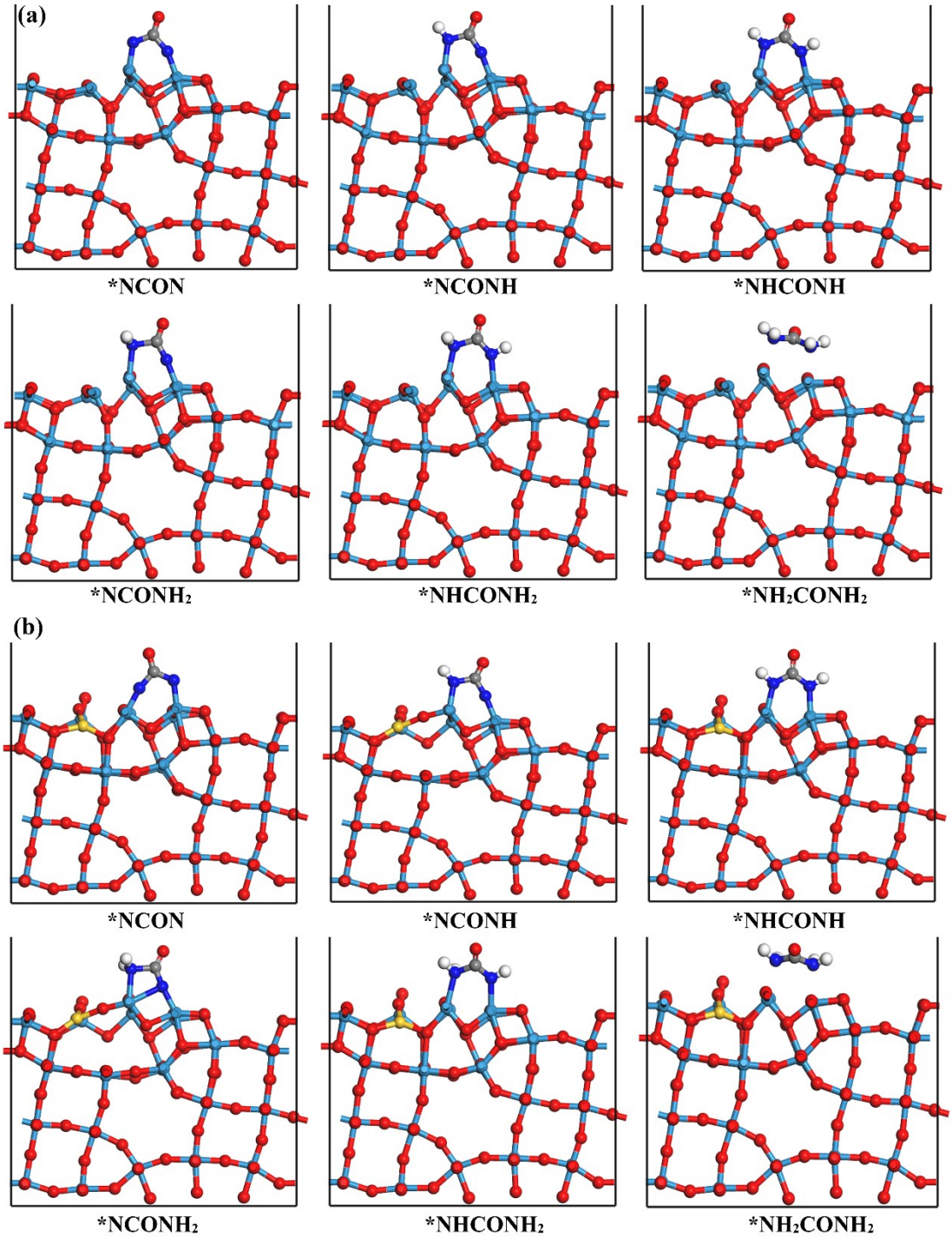

Fig. S19 Optimized structures of various intermediates for urea production on the (a) $W_{18}O_{49}$ and (b) Cu-$W_{18}O_{49}$-a.

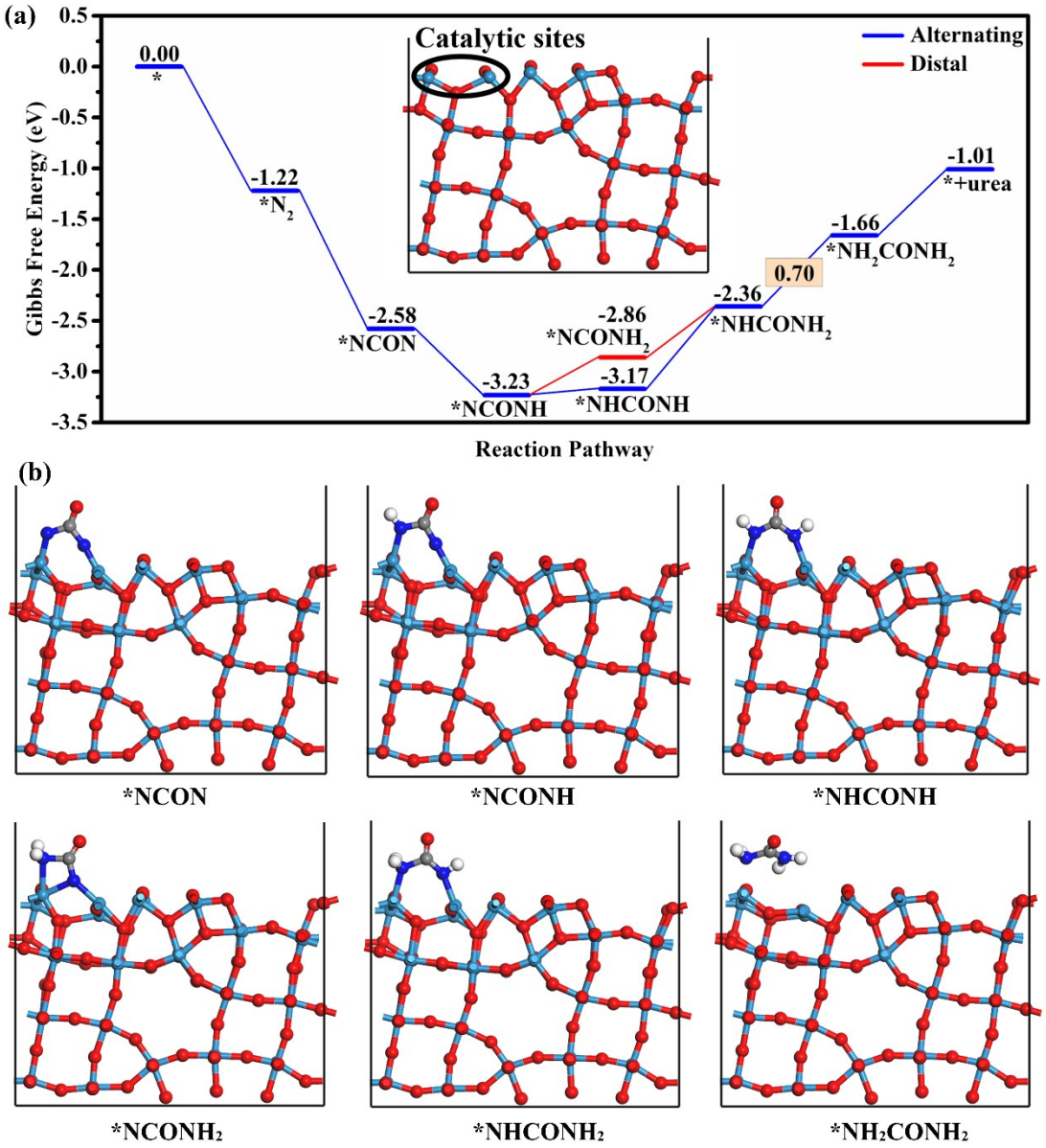

Fig. S20 (a) Gibbs free energy diagram and (b) optimized structures of various intermediates for urea production on the site $*N_2$-a of $W_{18}O_{49}$.

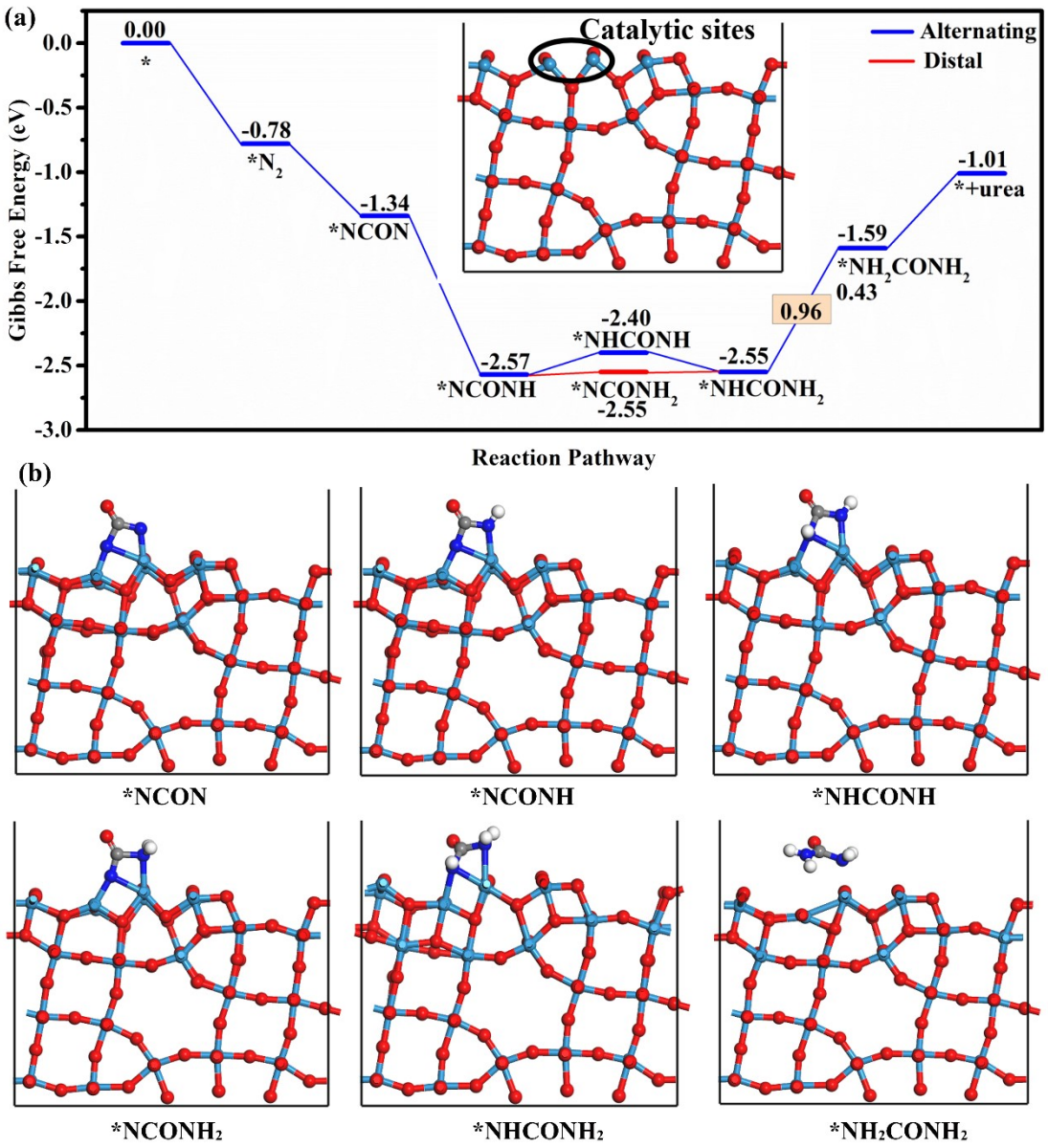

Fig. S21 (a) Gibbs free energy diagram and (b) optimized structures of various intermediates for urea production on the site $*N_2$-b of $W_{18}O_{49}$.

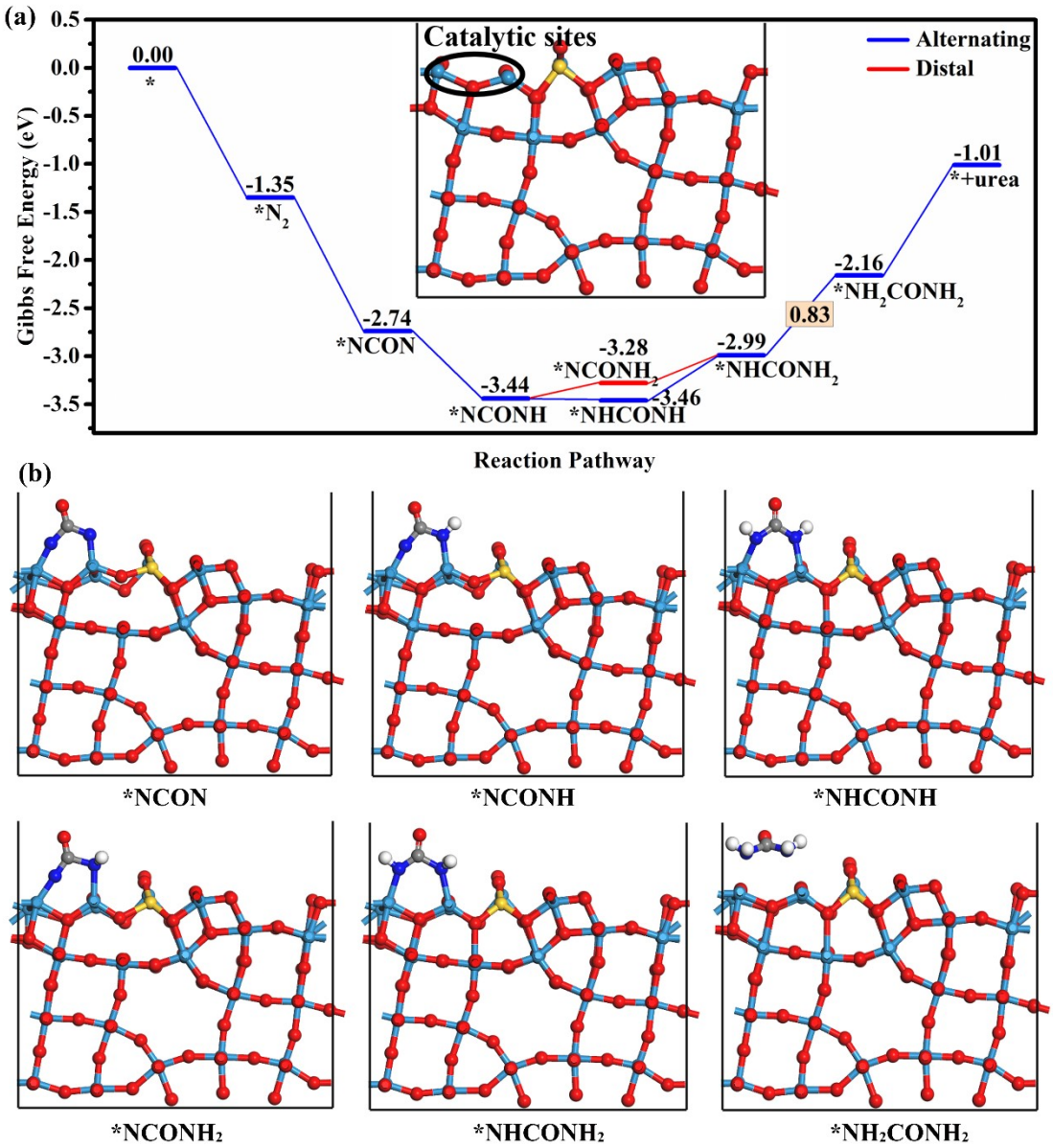

Fig. S22 (a) Gibbs free energy diagram and (b) optimized structures of various intermediates for urea production on the site $*N_2$-g of Cu-$W_{18}O_{49}$-b.

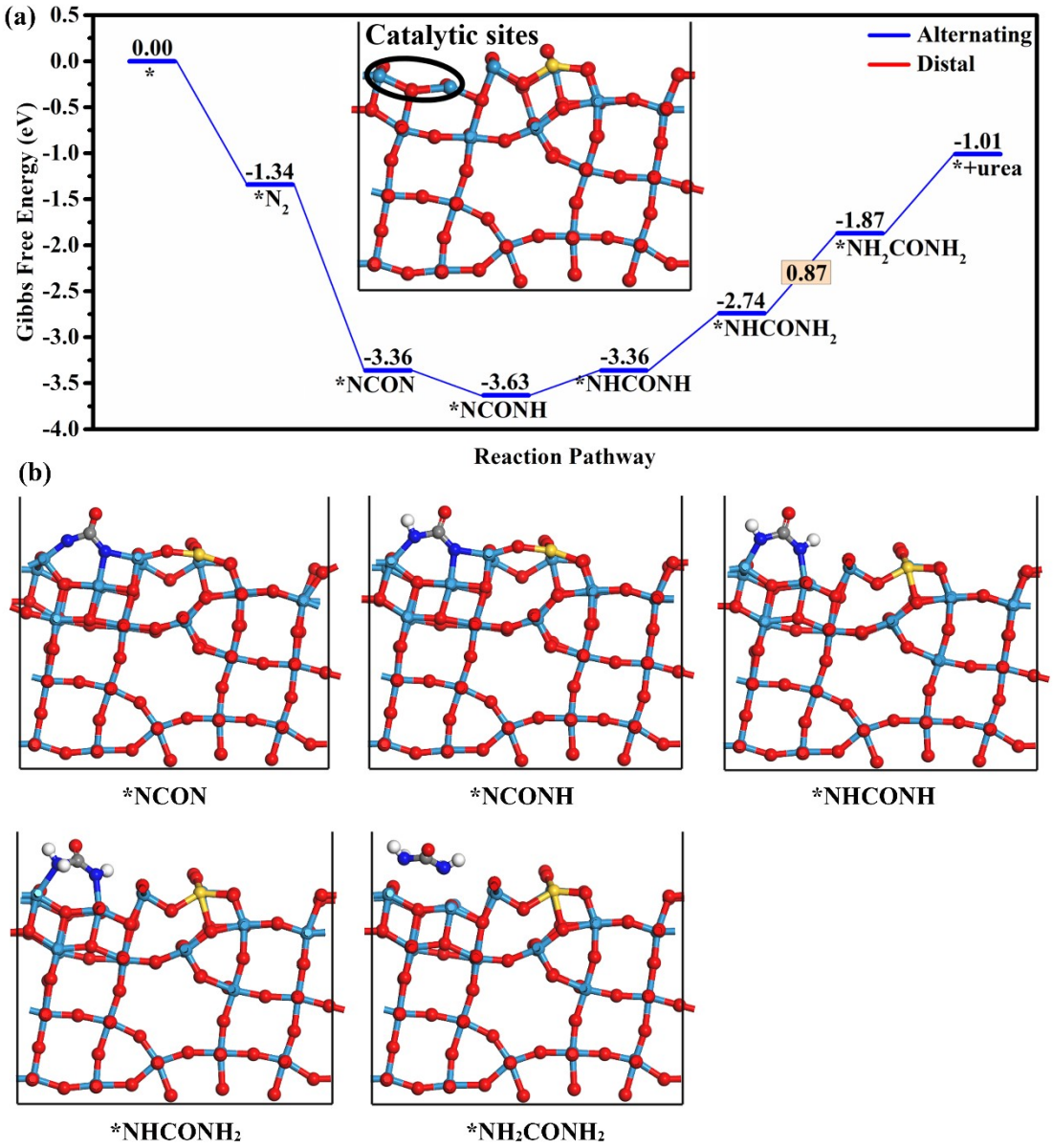

Fig. S23 (a) Gibbs free energy diagram and (b) optimized structures of various intermediates for urea production on the site $*N_2$-j of Cu-$W_{18}O_{49}$-c.

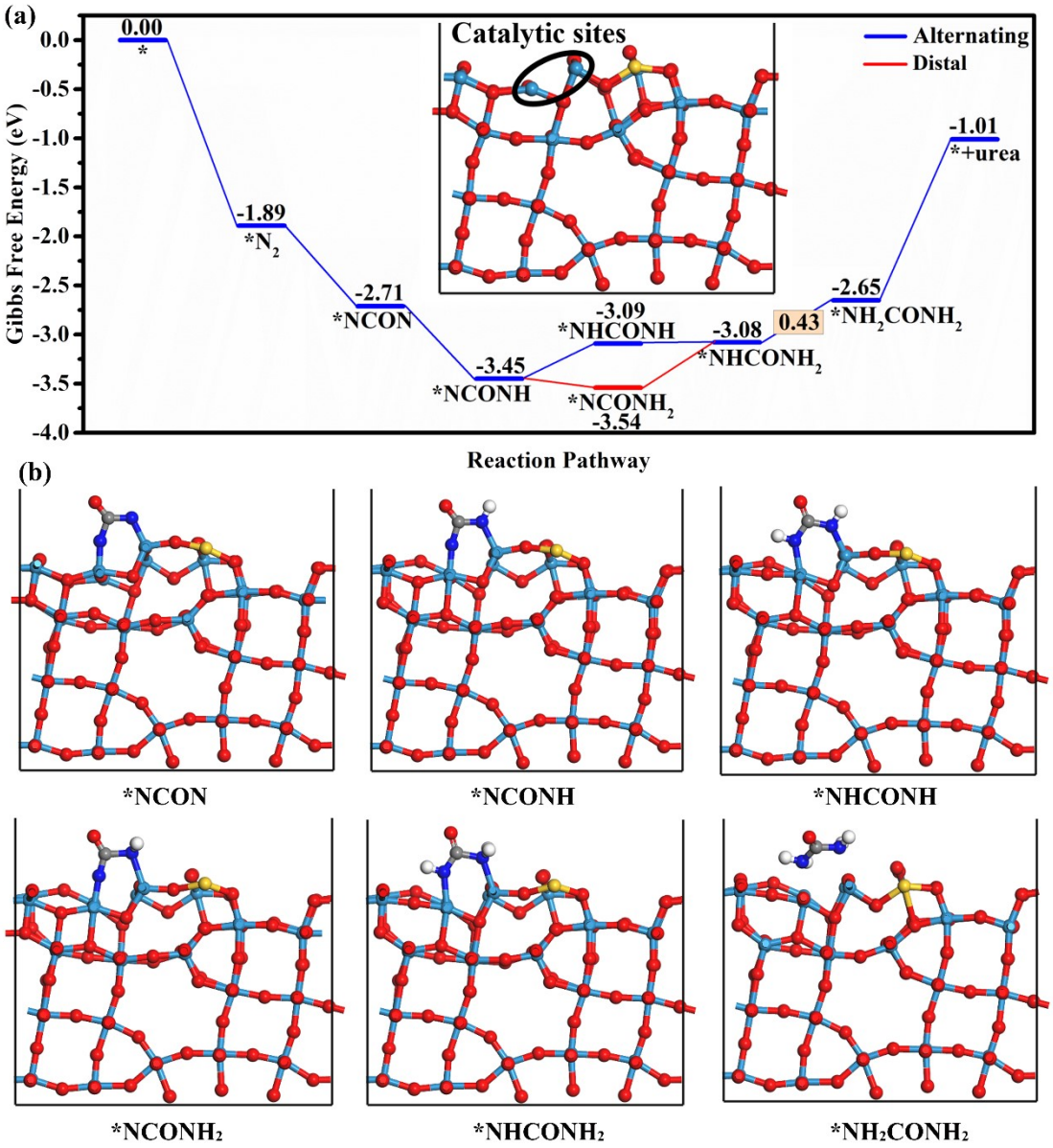

Fig. S24 (a) Gibbs free energy diagram and (b) optimized structures of various intermediates for urea production on the site $*N_2$-k of Cu-$W_{18}O_{49}$-b.

Table S3. The weight ratio of Cu, W and Zn in Cu-$W_{18}O_{49}$@ZIF-8

Cu (wt%)	W (wt%)	Zn (wt%)
0.37	4.17	6.52

Table S4. Comparison of urea yield rate and FEs among $W_{18}O_{49}$@ZIF-8 and other reported urea synthesis electrocatalysts

Catalysts	$V_{N_2} : V_{CO_2}$	Urea yield (mmol g^{-1} h^{-1})	Faradaic Efficiency (%)	ref
Cu-Pd alloy	1:1	3.36	8.92	34
Bi-$BiVO_4$	1:1	5.91	12.55	35
$BiFeO_3$/$BiVO_4$	1:1	4.94	17.18	36
$Ni_3(BO_3)_2$	1:1	9.7	20.36	37
InOOH	1:1	6.85	20.97	38
Co-PMDA-2-mnIM	1:1	14.5	48.97	39
CuPc NTs	1:1	2.39	12.99	40
MoP	1:1	0.206	36.5	41
PPy-coated Pt	1:1	2.4		42
Cu_1Pd_1-TiO_2	1:1	166.67 $mol_{urea}mol_{Pd}^{-1}h^{-1}$	22.54	43
defective Cu-Bi	1:1	3.72	8.7 ± 1.7	44
V_N-Cu_3N-300	1:1	81 μg h^{-1} cm^{-2}	28.7	45
ZnMn-N,Cl	1:1	4	63.5	46
Fe-N-C	1:1	0.156	2.13	47
Bi_2S_3/N-RGO	1:1	4.4	7.5	48
$Sb_xBi_{1-x}O_y$	9:1	5.13	10.9	49
Cu^{III}-HHTP	1:1	7.78	23.09	50
Cu-$W_{18}O_{49}$@ZIF-8	Simulated flue gas	1.33	16.1	This work

Table S5. Computed Gibbs free energies (ΔG, eV) of reaction $*N_2 + CO \rightarrow *NCON$ and $*N_2 + H^+ + e^- \rightarrow *NNH$ on the different catalytic sites of $W_{18}O_{49}$ and $Cu_{18}O_{49}$-Cu.

Sites	ΔG ($*N_2 + CO \rightarrow *NCON$)	ΔG ($*N_2 + H^+ + e^- \rightarrow *NNH$)
$*N_2$-a on $W_{18}O_{49}$	-1.36	-0.01
$*N_2$-b on $W_{18}O_{49}$	-0.56	0.27
$*N_2$-c on $W_{18}O_{49}$	-1.35	-0.16
$*N_2$-e on Cu-$W_{18}O_{49}$-a	-0.03	-0.69
$*N_2$-f on Cu-$W_{18}O_{49}$-a	-0.49	0.10
$*N_2$-g on Cu-$W_{18}O_{49}$-b	-1.39	0.00
$*N_2$-h on Cu-$W_{18}O_{49}$-b	0.58	-0.73
$*N_2$-i on Cu-$W_{18}O_{49}$-b	0.99	0.09
$*N_2$-j on Cu-$W_{18}O_{49}$-c	-2.02	0.29
$*N_2$-k on Cu-$W_{18}O_{49}$-c	-0.82	0.32
$*N_2$-l on Cu-$W_{18}O_{49}$-c	0.86	-0.48

Reference

[1] M. Rahmatullah; T. R. C., Clin. Chim. Acta, 1980, **107**, 3.
[2] Zhu, D.; Zhang, L.; R. E. Ruther, R. J. Hamers, Nat. Mater. 2013, **12**, 836.
[3] D. Singh, J. Ashkenazi, Phys. Rev. B, 1992, **46**, 11570.
[4] B. Barbiellini; M. Puska; T. Korhonen; A. Harju; T. Torsti; R. Nieminen, Phys. Rev. B, 1996, **53**, 16201.
[5] P. Blöchl, Phys. Rev. B, 1994, **50**, 17953.
[6] G. Kresse, G. Joubert, Phys. Rev. B, 1999, **59**, 1758.
[7] S. Grimme, J. Comput. Chem., 2006, **27**, 1787.
[8] a) J. Nørskov, J. Rossmeisl, A. Logadottir, L. Lindqvist, J. Kitchin, T. Bligaard, H. Jónsson,J. Phys. Chem. B, 2004, **108** 17886.
[9] J. Rossmeisl, A. Logadottir, J. Nørskov, Chem. Phys., 2005, 319178.